

Journal of Visualized Experiments

In vivo two-photon imaging of megakaryocytes and proplatelets in the mouse skull bone marrow --Manuscript Draft--

Article Type:	Invited Methods Collection - JoVE Produced Video
Manuscript Number:	JoVE62515R2
Full Title:	In vivo two-photon imaging of megakaryocytes and proplatelets in the mouse skull bone marrow
Corresponding Author:	Catherine Léon UMR_S1255 Strasbourg, FRANCE
Corresponding Author's Institution:	UMR_S1255
Corresponding Author E-Mail:	catherine.leon@efs.sante.fr
Order of Authors:	Alicia Bornert François Lanza Christian Gachet Catherine Léon
Additional Information:	
Question	Response
Please indicate whether this article will be Standard Access or Open Access.	Standard Access (US\$2,400)
Please specify the section of the submitted manuscript.	Biology
Please indicate the city, state/province, and country where this article will be filmed . Please do not use abbreviations.	France
Please confirm that you have read and agree to the terms and conditions of the author license agreement that applies below:	I agree to the Author License Agreement
Please provide any comments to the journal here.	
Please indicate whether this article will be Standard Access or Open Access.	Standard Access (\$1400)

TITLE:

In Vivo Two-photon Imaging of Megakaryocytes and Proplatelets in the Mouse Skull Bone Marrow

AUTHORS AND AFFILIATIONS:

Alicia Bornert¹, François Lanza¹, Christian Gachet¹, Catherine Léon¹

¹Université de Strasbourg, INSERM, EFS Grand Est, BPPS UMR-S 1255, FMTS, F-67000 Strasbourg, France

Email addresses of co-authors:

Alicia Bornert	alicia.bornert67@gmail.com
François Lanza	francois.lanza@efs.sante.fr
Christian Gachet	christian.gachet@efs.sante.fr

Corresponding author:

Catherine Léon catherine.leon@efs.sante.fr

KEYWORDS:

Two-photon microscopy; Intravital observation; Skull Bone marrow; Megakaryocytes; Proplatelets

SUMMARY:

We describe here the method for imaging megakaryocytes and proplatelets in the marrow of the skull bone of living mice using two-photon microscopy.

ABSTRACT:

Platelets are produced by megakaryocytes, specialized cells located in the bone marrow. The possibility to image megakaryocytes in real time and their native environment was described more than 10 years ago and sheds new light on the process of platelet formation. Megakaryocytes extend elongated protrusions, called proplatelets, through the endothelial lining of sinusoid vessels. This paper presents a protocol to simultaneously image in real time fluorescently labeled megakaryocytes in the skull bone marrow and sinusoid vessels. This technique relies on a minor surgery that keeps the skull intact to limit inflammatory reactions. The mouse head is immobilized with a ring glued to the skull to prevent movements from breathing.

Using two-photon microscopy, megakaryocytes can be visualized for up to a few hours, enabling the observation of cell protrusions and proplatelets in the process of elongation inside sinusoid vessels. This allows the quantification of several parameters related to the morphology of the protrusions (width, length, presence of constriction areas) and their elongation behavior (velocity, regularity, or presence of pauses or retraction phases). This technique also allows simultaneous recording of circulating platelets in sinusoid vessels to determine platelet velocity and blood flow direction. This method is particularly useful to study the role of genes of interest

in platelet formation using genetically modified mice and is also amenable to pharmacological testing (study the mechanisms, evaluating drugs in the treatment of platelet production disorders). It has become an invaluable tool, especially to complement *in vitro* studies as it is now known that *in vivo* and *in vitro* proplatelet formation rely on different mechanisms. It has been shown, for example, that *in vitro* microtubules are required for proplatelet elongation per se. However, *in vivo*, they serve as a scaffold, elongation being promoted by blood flow forces.

INTRODUCTION:

Platelets are produced by megakaryocytes—specialized cells located in the bone marrow. The precise way megakaryocytes release platelets in the circulation has long remained unclear owing to the technical challenge in observing real-time events through the bone. Two-photon microscopy has helped overcome this challenge and led to major advances in understanding the platelet formation process. The first *in vivo* megakaryocyte observations were made by von Andrian and colleagues in 2007, with the visualization of fluorescent megakaryocytes through the skull¹. This was possible because the bone layer in the frontoparietal skull of young adult mice has a thickness of a few tens of microns and is sufficiently transparent to allow visualization of fluorescent cells in the underlying bone marrow².

Ensuing studies applied this procedure to evaluate proplatelet formation under various conditions and to decipher the underlying mechanisms³⁻⁶. These studies provided definitive evidence that megakaryocytes dynamically extend protrusions, called proplatelets, through the endothelial barrier of the sinusoid vessels (**Figure 1**). These proplatelets are then released as long fragments that represent several hundred platelets in volume. The platelets will be formed after the remodeling of the proplatelets in the microcirculation of downstream organs, notably in the lungs⁷. To date, however, the precise process and molecular mechanisms remain subject to debate. For instance, the proposed role of the cytoskeletal proteins in the elongation of proplatelets differs between *in vitro* and *in vivo* conditions³, and differences in proplatelet formation have been demonstrated under inflammatory conditions⁶. Complicating things further, a recent study disputed the proplatelet-driven concept and proposed that *in vivo*, platelets are essentially formed through a membrane-budding mechanism at the megakaryocyte level⁸.

This paper presents a protocol for the observation of megakaryocytes and proplatelets in the bone marrow from the skull bone in living mice, using a minimally invasive procedure. Similar approaches have been previously described to visualize other marrow cells, notably hematopoietic stem and progenitor cells⁹. The focus here is on the observation of megakaryocytes and platelets to detail some parameters that can be measured, notably proplatelet morphologies and platelet velocity. This protocol presents how to insert a catheter into the jugular vein to inject fluorescent tracers and drugs and observe through the skull bone. The calvarial bone is exposed using minor surgery so that a ring is glued to the bone. This ring serves to immobilize the head and prevent movements due to breathing and form a cup filled with saline as the immersion medium of the lens. This technique is well suited to i) observe in real time the sinusoid geometry and megakaryocytes interacting with the vessel wall; ii) follow megakaryocytes in the process of proplatelet formation, elongation, and release; and iii) measure

platelet movements to monitor the complex sinusoid blood flow. Data obtained using this protocol have been recently published³.

PROTOCOL:

All animal experiments were performed in accordance with European standards 2010/63/EU and the CREMEAS Committee on the Ethics of Animal Experiments of the University of Strasbourg (Comité Régional d’Ethique en Matière d’Expérimentation Animale Strasbourg).

1. Preparation of mice and insertion of a catheter in the jugular vein

NOTE: Here, male or female, 5–7-week-old mTmG reporter mice were used (B6.129(Cg)-*Gt(ROSA)26Sor^{tm4}(ACTB-tdTomato,-EGFP)^{Luo10}*) crossed with Pf4-cre mice¹¹, allowing intense green fluorescence labeling in megakaryocytes and platelets¹². Before beginning the experiment, preheat the heating chamber of the microscope for a few hours.

1.1. Transport the mouse to the imaging room and proceed to anesthesia.

1.1.1. Anesthetize the mouse by intraperitoneal (i.p.) injection of a solution of ketamine (ketamine (100 µg/g) and xylazine (10 µg/g) (5 µL/g).

NOTE: Repeated administration of ketamine/xylazine is used here and works well but requires the interruption of recording for regular reinjection. Alternatively, if an anesthesia machine is available, the induction of anesthesia may be performed with ketamine/xylazine and subsequently maintained under inhalation of gases (mixture of isoflurane, air, and oxygen).

1.1.2. Replace the animal in its cage until it reaches deep anesthesia. Place the mouse on a heated plate warmed at 37 °C for all subsequent manipulations.

NOTE: While the animal reaches deep anesthesia, switch on the microscope and all equipment (see section 4.1) and set up the different parameters needed (see section 4.2) to start the experiment once the surgery is done.

1.2. Install a catheter in the jugular vein.

NOTE: It is important to avoid microbial contamination during the surgery as far as possible. Take care to carefully disinfect the skin with 70% ethanol (EtOH) before proceeding with surgery. Always use sterilized scissors and tweezers, and regularly rinse them in 70% EtOH. Work in a clean place, and wear a face mask. A 22 G “over-the needle” catheter, consisting of a needle inside a plastic tube, is used for intravenous injection (see the **Table of Materials**).

1.2.1. Place the mouse on its back, and fix the anterior legs with surgical tape to stretch the throat (**Figure 2A**). Disinfect the throat with 70% ethanol.

1.2.2. Make a 0.7–1 cm incision over the right or left jugular vein using sterile scissors. Stretch the adjacent connective tissue to expose the external jugular vein and the top of the pectoral muscle (**Figure 2B**).

1.2.3. Fill the catheter with warm, sterile physiological saline. Insert the catheter into the vein after penetrating through the pectoral muscle (**Figure 2C**).

NOTE: Take care to avoid air bubbles inside the catheter. It is important to insert the catheter through the muscle to prevent hemorrhage as the muscle will form a compression point. Even mice with hemostasis defects, such as *Itgb3*^{-/-} mice, do not bleed upon catheter insertion with this approach.

1.2.4. Gently remove the needle, and if required, carefully move the catheter deeper into the vein. Stabilize the catheter by adding a drop of surgical glue (**Table of Materials**).

NOTE: It is possible to insert the catheter inside the tail vein, although it requires some practice as the vein has a small caliber, especially when using mice with dark hair. In that case, dilate the vein by warming the tail under an infrared lamp or through immersion in warm water. Due to its larger caliber, positioning the catheter inside the jugular vein may allow larger volumes or repeated treatments to be injected more reliably.

1.2.5. Carefully return the mouse to a prone position. Apply gel (**Table of Materials**) on the eyes to prevent dryness.

2. Surgery and installation of the cranial ring

NOTE: The full support for mouse installation comprises 4 pieces, a block and a plate, the ring to hold the mouse head, and a screw to fix the ring to the block (**Figure 3A**). All elements of the support have been obtained from i.materialise.com by 3D printing. The plate is made of acrylonitrile butadiene styrene (ABS) polymer, the block and screw of stainless steel, and the ring of high-grade stainless steel (high-detailed stainless steel) (See **Supplemental Figure S1** for dimensions and **Supplemental Materials** for the 3D printing files). The block is fixed permanently to the support, either screwed or glued. Once the ring is fixed on the mouse skull, it should be screwed to the block holder (**Figure 3A**).

2.1. Moisten the hair on the scalp with a paper towel wet with 70% ethanol for disinfection. Remove all the loose hair with a wet paper towel.

NOTE: For convenience, the scalp may be shaved before surgery.

2.2. Incise the scalp by forming a T at the midline up to 1 cm and between the ears to expose the calvarium using sterile fine scissors and tweezers (**Figure 3B**).

NOTE: The ring will be positioned to overlap the frontal and parietal bones (**Figure 3C**).

2.3. Use sterile tweezers to expose the skull. Carefully remove the periosteum with scissors and tweezers. Use a sterile cotton swab soaked with physiological saline to remove all the periosteum and any debris or hair, which could alter imaging.

NOTE: To limit inflammatory reactions, take great care not to damage the bone.

2.4. Remove any blood traces by rinsing with saline, and rapidly dry the bone with a dry cotton swab. Apply the glue gel to the ring, position it on the exposed bone, and maintain it for a few seconds so that the ring is firmly attached to the skull (**Figure 3D**).

NOTE: No glue must enter the observation field as it may lead to undesirable autofluorescence.

2.5. Lightly moisten the skull with a cotton swab immersed in physiological saline.

2.6. Prepare the silicon dental paste by carefully mixing 1:1 blue and yellow components. Apply dental paste all around the ring for sealing to prevent leakage during imaging. Carefully remove any dental paste or glue that may have entered the ring.

2.7. Fill the ring with saline and check for leakage.

NOTE: The saline serves as the immersion medium for the microscope objective. Bleeding may be more critical when using mice with hemostasis-related defects. It is essential to prevent blood from entering the ring as it may blur further imaging.

2.8. Place the mouse on the support, and screw the ring on the block holder (**Figure 3C**). Place folded compresses under the animal's head to raise the head and prevent detachment of the ring from the skull.

NOTE: The head is directly fixed so that it prevents image movements due to breathing.

2.9. Position the support and mouse assembly in the heated microscope chamber (**Figure 3G**).

NOTE: Be careful not to dislodge the inserted catheter at any time.

3. Follow-up of the anesthetized mice until the end of the experiment

NOTE: Anesthesia is re-induced every 35 min by alternating subcutaneous (s.c.) injections of ketamine (25 µg/g) in a volume of 5 µL/g body weight and a mixture of ketamine (50 µg/g) and xylazine (5 µg/g) (1.2 µL/g).

3.1. If required, stop acquisition and re-induce anesthesia by s.c. injection.

3.1.1. Being careful not to move the mouse head, pinch the skin of the back between the thumb

and index finger of the left hand. Subcutaneously inject the anesthetic in the fold of the back skin using the right hand (or *vice versa* for left-handed people).

3.2. Check for the presence of saline in the ring, and if necessary, fill with fresh saline. Go on recording for the next 35 min, and proceed similarly for the recording duration.

3.3. At the end of the experiment, euthanize the mouse by cervical dislocation before it wakes up.

NOTE: The mouse is kept anesthetized for a maximum duration of 3 h, in agreement with the local ethical and animal welfare committee.

4. Two-photon imaging

NOTE: See the **Table of Materials** for details about the microscope and related equipment. Images were recorded with a resonant scanner (12 or 8 kHz). The bidirectional mode was set up to increase speed acquisition as pixels are recorded in both directions; hence, any mismatch in the phase must be corrected with the control panel “phase correction.” Finally, an adapted averaging was set up as a compromise between speed of acquisition and signal-to-noise ratio.

4.1. Switch on the two-photon microscope, including the laser and resonant scanner (output laser power usually ~1.8–2.5 W depending on the laser).

4.2. Set the appropriate laser wavelength for the chosen fluorophores. Set the appropriate wavelength for the recovery of emitted lights.

NOTE: Here, a wavelength of 913 nm and hybrid detectors (500–550 nm and 575–625 nm) were used to simultaneously excite and detect AlexaFluor-488 and Qtracker-655, respectively.

4.3. Using the intrajugular catheter, inject the fluorescent tracer to label the vasculature (Qtracker-655; **Table of Materials**). Inject 50 μL /mouse of a solution at 0.2 μM , renewed once every hour for a maximum of 150 μL /experiment.

NOTE: Other tracers can be used such as high molecular weight dextran¹. In that case, consider that blood viscosity can be altered by dextran and modify some hemorheological parameters.

4.4. Place the microscope stage with the support and mouse under the objective of the microscope. Check that the ring is always filled with saline and immerse the objective. Use epifluorescence to locate the bone marrow vessels (red) and the presence of megakaryocytes (green) aligned along sinusoid vessels.

NOTE: The skull bone has a thickness lower than 100 μm^2 . The marrow is located beneath the bone and is easily recognized by the fluorescent green megakaryocytes and the dense red anastomosed sinusoid vessels labeled by Qtracker-655.

4.5. Long acquisitions (megakaryocytes, proplatelets)

4.5.1. Search for the region of interest. Apply image acquisition parameters as mentioned above.

4.5.2. For long acquisitions (e.g., visualization of proplatelet formation or elongation), acquire z-stack images at 1.34 μm intervals using an 8 kHz resonant scanner.

NOTE: A 12 kHz resonant scanner can increase acquisition speed.

4.5.3. Acquire 384 x 384 pixel images to visualize the entire megakaryocyte and vessel. Use line averaging, as desired, for rapid acquisition with good resolution. Determine the time interval of image stack acquisition, usually 10 s or 30 s for proplatelet visualization.

NOTE: Here, a line averaging of 8 was used to obtain a higher signal-to-noise ratio, which allowed the acquisition of 1 image/10 s with an 8 kHz resonant scanner.

4.6. Short and rapid acquisition (platelets)

NOTE: For shorter acquisition of rapid events, such as platelet velocity, it is essential to maximize the frame acquisition rate.

4.6.1. Minimize (e.g., 256 x 90 pixels) and adjust image size to the vessel by rotating the imaging field, if required.

4.6.2. Use the highest available scanning speed.

4.6.3. Use bidirectional scanning.

NOTE: For bidirectional scanning, ensure that the phase is well-adjusted.

4.6.4. Minimize line averaging to find the optimal compromise between image definition and rapidity of acquisition.

NOTE: For platelet velocity measurements, a pixelized image may be sufficient if it helps increase the rapidity of acquisition.

4.6.5. Minimize z-stack to increase acquisition rapidity. Acquire only 1 z-stack, and follow the same platelet for a few images. Acquire for 10–20 s to measure platelet velocity.

NOTE: A maximum of 133 frames/s can be obtained using these conditions with a 12 kHz resonant scanner. The parameters must be adapted to the conditions. In some vessels, platelet velocity is nevertheless too high to quantify platelet velocity with these settings reliably.

4.7. Proplatelet width and length measurement

NOTE: To load LIF-files obtained on Leica software with ImageJ, first download and install the LOCI plug-in on ImageJ to use the Bio-Formats Importer.

4.7.1. Proplatelet width

4.7.1.1. Open the movie with ImageJ. To perform width measurement, use only the movie of the proplatelets without the vessel. To separate the different channels, click on **Image | Color** and select **Split Channels**.

4.7.1.2. For a z-stack movie, make an average z-projection for each time point by clicking on **Image | Stacks** and select **Z Project**. For **Projection type**, enter **average Intensity**.

4.7.1.3. Treat the image to remove the noise. Subtract the background by clicking on **Process | Subtract background** and apply **Rolling ball radius: 50.0 pixels**. Smooth the image by clicking on **Process and Smooth**.

4.7.1.4. Trace a line close to the base of the proplatelet (near the megakaryocyte, avoiding any other object).

NOTE: Do not forget to set the scale of the image to obtain the value in the desired unit by clicking on **Analyze and Set Scale**. By default, the unit of the image is in pixels.

4.7.1.5. Plot the intensity profile, fit a gaussian curve, and calculate the Full Width at Half Maximum (FWHM). For that, write the following script in a macro by clicking on **Plug-ins | New** and select **Macro** and run it: `y=getProfile(); x=Array.getSequence(y.length); Fit.doFit("Gaussian",x,y); Fit.plot(); sigma=Fit.p(3); FWHM = (2 * sqrt(2 * log(2))) * sigma; print(FWHM).`

NOTE: Ensure that there is only a single peak in the line scan, corresponding to the proplatelet intensity.

4.7.1.6. Perform the actions described in step 4.7.5 on 1 slice or repeated over time to get the mean width of the proplatelet

4.7.2. Proplatelet length

4.7.2.1. Trace a line along the proplatelet, from the base close to the megakaryocyte to the top. Use a segmented line to follow the proplatelet shape. Repeat it for each time point.

4.7.2.2. Remember to save each line using the ROI Manager: click on **Analyze | Tools** and select **ROI Manager**. Click on **Add** in the **ROI Manager** window to add each line to the manager

as is it selected. To save all the lines in a folder, click in the **ROI Manager** on **Deselect | More** and click on **Save**. From the ROI Manager, extract the length value of each line (**Measure**) from the results table.

NOTE: Do not forget to set the scale of the image to obtain the value in the desired units by clicking on **Analyze and Set Scale**. By default, the unit of the image is in pixels.

4.8. Platelet velocity measurement

NOTE: Platelet velocity is calculated from the video recording of fluorescent platelets flowing inside the vessel over 10–20 s. A first-image treatment is performed to obtain cyclically repeated line-scan data. Motion leads to streaks whose angle depends on the velocity, allowing its calculation. Here, velocity was calculated with a method that uses the Radon transform, which is more robust than the classical Singular Value Decomposition (SVD) method¹⁵.

4.8.1. Image treatment with ImageJ

4.8.1.1. Open the movie with ImageJ. Apply a Gaussian Blur filter by clicking on **Process | Filters**, select **Gaussian Blur**, and apply **Sigma (Radius): 2.00**. Choose a small region to measure the flow, and trace 3 adjacent lines following the flow direction.

NOTE: Do not forget to save each line by using the ROI Manager by clicking on **Analyze | Tools | ROI Manager**. Click on **Add** in the **ROI Manager** window to add each line and save them; click first on **Deselect | More** and then click on **Save**.

4.8.1.2. Using ImageJ line-scan software, build a kymograph for each line by clicking on **Image | Stacks**; select **Reslice** and apply the following parameters: **Output spacing (microns): 1.000 / Slice count: 1 / Avoid interpolation**. Save the resulting space-time images.

NOTE: The resulting image shows streaks corresponding to the linear motion of the platelets in the blood flow over time. The angle of a streak is a function of the velocity.

4.8.2. Velocity measurement using Matlab or GNU Octave software

NOTE: The velocity of the platelets in the blood flow is estimated from the space-time images using a computational analysis method based on the Radon transform described by Drew and collaborators¹⁵. The description of this mathematical method is beyond the scope of this review, and the reader is referred to the publication by Drew et al. for details regarding the calculation¹⁵. Both the Matlab code and more information are available on their website <https://www.drew-lab.org/code>.

4.8.2.1. Open the code using Matlab or GNU Octave software.

NOTE: The code may require adaptation according to the desired study.

4.8.2.2. Extract the value from the 3 space-time images, corresponding to the adjacent lines drawn in the same vessel portion. Calculate the mean platelet flow velocity value for this portion of the vessel.

NOTE: Do not forget to convert the result in the correct unit of measure (e.g., $\mu\text{m/s}$).

REPRESENTATIVE RESULTS:

Using this protocol, the fluorescent tracer, Qtracker-655, was intravenously administered to image anastomosed marrow sinusoid vessels in the skull bone marrow and the flow direction as depicted by the arrows (**Figure 4A**, left). Using mTmG mice, eGFP-fluorescent platelets were recorded over 20 s in each vessel branch, and their velocity was measured using ImageJ and GNU Octave software (**Figure 4A**, right). Note the heterogeneity in flow velocity and direction. Sinusoid vessels present complex flows due to the anastomoses, with the presence of flow-reflow and even stasis, as shown in the bifurcation recorded in **Video 1**. The same bifurcation is shown in **Figure 4B** (left), with the red and blue arrows highlighting opposite flows. Platelet velocity in this bifurcation has been measured and reported in the graph (**Figure 4B**, right). The red tracing corresponds to the velocity in the left vessel branch and the blue tracing to that in the right vessel branch. This shows irregularity over time in each vessel branch, with phases of acceleration, stasis, and deceleration. It is important to note that in some vessels, blood flow was too rapid for reliable analysis under the present acquisition conditions.

Proplatelet elongation recording allows the visualization of their various morphologies over time (**Figure 5**). Some proplatelets elongate with irregular morphologies (**Figure 5Ai** and **Video 2**). Others, usually thinner ones, may extend over long distances necessitating the movement of the acquisition window to follow their extension (**Figure 5Aii** and **Supplemental Video 1**). Others are shorter and thicker and usually elongate slowly (**Figure 5Aiii** and **Supplemental Video 2**). When megakaryocytes extend proplatelets in areas of complex flows, such as the bifurcation shown in **Figure 4B**, proplatelets are tossed from one vessel branch to the other according to flow direction (**Figure 5B** and **Video 3**). The importance of hemodynamic forces for proplatelet elongation in the flow direction was evidenced when the mouse unexpectedly underwent cardiac arrest. Stopping blood flow relaxed the proplatelets extended by the megakaryocyte (**Figure 5C** and **Video 4**).

When the quality/resolution of acquisition is appropriate, morphological parameters can be measured, such as the length of proplatelets until detachment, their width at the base of the proplatelet or any other defined location, or the size of the buds (**Figure 6A**). A mean maximal proplatelet length of $\sim 185 \mu\text{m}$ (range $41.5\text{--}518.5 \mu\text{m}$) and a mean proplatelet width of $5.2 \mu\text{m}$ (range $2.8\text{--}8 \mu\text{m}$) was calculated (**Figure 6A**). Plotting proplatelet length as a function of time allows the visualization of the behavior of proplatelets during phases of elongation, stasis, or even retraction (**Figure 6B**). Measurement of proplatelet elongation velocity is an important parameter, which directly reflects the elongation, stasis, or retraction behavior of proplatelets³.

Proplatelet elongation velocity can be measured if the proplatelet remains attached to its mother

cell; once detached, it will be immediately carried away by the flow and disappear from the visualization window. In wild-type (WT) mice, the mean proplatelet elongation velocity was $\sim 10 \mu\text{m}/\text{min}$ (**Figure 6C**), in agreement with previous publications¹. Finally, it is possible to inject drugs through the catheter inserted in the jugular vein. For instance, it has been observed that intravenous administration of vincristine, a drug that depolymerizes microtubules, led to the retraction of proplatelets from WT mice but had no effect on proplatelets from myosin IIA-deficient mice (*Myh9*^{-/-}) (**Video 5** and **Video 6**)³.

FIGURE AND TABLE LEGENDS:

Figure 1: Schematic representation of proplatelet formation in the bone marrow. After differentiation from hematopoietic stem cells, large megakaryocytes align along sinusoid vessels and extend cytoplasmic projections, called proplatelets, through the endothelial barrier. Proplatelets elongate and detach under the influence of hemodynamic forces to further remodel into platelets in the downstream microcirculation.

Figure 2: Insertion of the catheter. (A) An incision is made to expose the jugular vein and the top of the pectoral muscle. (B) The catheter filled with saline is inserted in the jugular vein by passing through the muscle, creating a compression point. (C) The mouse is carefully turned so that it lies ventral surface downward with the catheter well-positioned.

Figure 3: Experimental setup used for two-photon imaging through the skull bone. (A) The 3D printed stainless steel block is fixed on the ABS polymer support (see **Supplemental Figure S1** and **Supplemental Materials** for the 3D designs). The block and the skull ring are designed so that the ring can be screwed to the block. Note that, for ease of use, the screw head has been embedded in Epon. (B) Schematic showing the positioning of the ring on the exposed skull bone. (C) Photographs illustrating the mouse with the ring glued to the skull, the head on a tissue pad, and (D) the positioning under the microscope objective. Abbreviations: 3D = three-dimensional; ABS = acrylonitrile butadiene styrene.

Figure 4: Measure of platelet velocity in skull bone marrow anastomosed sinusoid vessels. (A) Left, two-photon imaging of sinusoid vessels labeled by Q-Dot injection. z-projection showing the anastomosis of the sinusoid vessels in the skull bone marrow. Arrows indicate the direction of flow, illustrating the complexity of the flows in sinusoids. Right, mean flow velocity estimated by the measurement of the platelet velocity in each vessel branch. The numbers on the x-axis correspond to the arrow numbers in the image on the left. (B) Left, sinusoid bifurcation delineated by dotted lines, showing platelets flowing in opposite directions (red and blue arrows) (corresponding to **Video 1**). Two-photon single plane image. Right, a graph showing the flow velocity in each portion of the vessel as a function of time (red line, left side; blue line, right side), showing phases of stasis, acceleration, and deceleration. Scale bars = $20 \mu\text{m}$.

Figure 5: Various proplatelet morphologies observed in the skull marrow by two-photon microscopy. (A) Three representative *in vivo* proplatelets: z-projection images from time-lapse experiments (shown in **Video 2**, **Supplemental Video 1**, and **Supplemental Video 2**) showing the

various morphologies of proplatelets (arrows) extending within bone marrow sinusoids. Proplatelets and megakaryocytes are in green; sinusoid vessels are in red. **(B)** Time-lapse images of a proplatelet in the same bifurcation as in **Figure 4B**, oscillating according to the direction of flow (also shown in **Video 3**). **(C)** z-projection time-lapse images showing relaxation of 3 proplatelets after cessation of blood flow due to cardiac arrest of the mouse, previously aligned in the same flow line (indicated by the white, yellow, and blue arrows). Scale bars = 20 μm .

Figure 6: Proplatelet morphological analyses. **(A)** Upper, z-projection image depicting the site where the proplatelet width was measured along with maximal length; below are graphs representing the maximal length of 25 individual proplatelets and the mean proplatelet width of the same proplatelets (same gray code) throughout elongation. i) The proplatelet width was measured by drawing a perpendicular line at a fixed position close to the base of the proplatelet, and the profile intensity was recorded at this position every minute. A Gaussian curve was fitted to this profile, and the FWHM was considered to represent the width of the proplatelet. The mean width was then calculated by averaging the widths of the proplatelet measured at each time point at the fixed position. Bars are mean \pm sem of the width measured every minute during acquisition; ii) the maximal proplatelet length was also determined, from the base of the proplatelet to its tip. **(B)** Individual tracings showing the elongation behavior of WT proplatelets, some of them presenting pause and retraction phases. To better highlight the pauses and retractions upon the process of proplatelet growth, the length measured every 10 s was represented as a percentage of the maximal length of each proplatelet. **(C)** Scatter plot representing the proplatelet elongation speed. The net mean proplatelet elongation speed (including pauses and retractions) was calculated as the change in proplatelet length at 1 min intervals, averaged over the whole time sequence. Individual values and mean \pm sem. Abbreviations: FWHM = Full Width at Half Maximum; sem = standard error of the mean; WT = wild-type; Myh9 = myosin heavy chain 9.

Video 1: Reverse flow within sinusoid vessels. Circulating platelets (green) within the sinusoid vessels (red, Qtracker) (single confocal z-plane). An anastomosed sinusoid vessel is shown presenting bifurcations where the flow is unstable and displays phases of stasis, acceleration, and deceleration. Acquired with a Leica SP5 microscope equipped with a 12 kHz resonant scanner and a 25x water objective with a numerical aperture of 0.95 (Leica), one plane, 256 x 90 pixels, bidirectional acquisition, line averaging 2, 133 frame/s.

Video 2: Elongating proplatelets display various morphologies. Representative time-lapse video recording (z-projection) in a WT mouse with megakaryocytes extending proplatelets with various morphologies (green) within bone marrow sinusoids (red, Qtracker). Acquired with a Leica SP5 microscope equipped with a 12 kHz resonant scanner and a 25x water objective with a numerical aperture of 0.95 (Leica), z-stack acquisition at 10 s intervals, z-depth of 1.34 μm , x-y resolution 384 x 384 pixels, line averaging 8. Whenever necessary, the profiles were aligned using the ImageJ template matching plug-in to obtain an average z-projection. Depending on the image quality, the background was subtracted, the image was smoothed, and the brightness and contrast adjusted.

Video 3: Proplatelets are tossed by changes in the flow direction. Time-lapse video showing a wild-type megakaryocyte in the sinusoid bifurcation shown in **Video 1**, in the process of extending a proplatelet that oscillates in one vessel branch depending on the direction of flow (z-projection). Acquired with a Leica SP5 microscope equipped with a 12 kHz resonant scanner and a 25x water objective with a numerical aperture of 0.95 (Leica), z-stack acquisition at 10 s intervals, z-depth of 1.34 μm , x-y resolution 384 x 384 pixels, line averaging 8. The profiles were aligned using the ImageJ template matching plug-in, and an average z-projection was obtained. The background was subtracted, the image was smoothed, and the brightness and contrast adjusted.

Video 4: Impact of flow on proplatelet alignment and tension. Time-lapse video recording of a proplatelet before and after cardiac arrest. The video shows three proplatelets (green, labeled with AF-488 anti-GPIX antibody derivative) in the same flow line before cardiac arrest, thus poorly individualized at the resolution of the two-photon microscopy. Following cardiac arrest, the three proplatelets separate and become relaxed in the absence of blood flow. Video acquired with a Leica SP8 confocal microscope equipped with an 8 kHz resonant scanner, image with a 25x water objective with a numerical aperture of 0.95 (Leica). The profiles were aligned using the ImageJ template matching plug-in, and an average z-projection was obtained. The background was subtracted, the image was smoothed, and the brightness and contrast adjusted.

Video 5: Impact of vincristine drug injection on the proplatelet behavior of WT (mice. Time-lapse video recording of a proplatelet before and after administration of vincristine (1 mg/kg) (z-projection). The elongating proplatelet (green) within the sinusoid vessels (red) starts to retract after intravenous administration of vincristine. Video was acquired with a Leica SP8 confocal microscope equipped with an 8 kHz resonant scanner, image with a 25x water objective with a numerical aperture of 0.95 (Leica). The profile was aligned using the ImageJ template matching plug-in, and an average z-projection was obtained. The background was subtracted, the image was smoothed, and the brightness and contrast adjusted.

Video 6: Impact of vincristine drug injection on the proplatelet behavior of myosin-deficient mice. Time-lapse video recording of a proplatelet before and after administration of vincristine (1 mg/kg) (z-projection). The elongating proplatelet (green) within the sinusoid vessels (red) continues to elongate in the *Myh9*^{-/-} mice. Video was acquired with a Leica SP8 confocal microscope equipped with an 8 kHz resonant scanner, image with a 25x water objective with a numerical aperture of 0.95 (Leica). The profile was aligned using the ImageJ template matching plug-in, and an average z-projection was obtained. The background was subtracted, the image was smoothed, and the brightness and contrast adjusted.

Supplemental Figure S1: Design for the 3D printing of the skull ring and support. This design was used to 3D print (A) the skull ring in high-quality stainless steel, (B) the screw, (C) the block in stainless steel, and (D) the support in ABS polymer. Abbreviations: 3D = three-dimensional; ABS = ABS = acrylonitrile butadiene styrene.

Supplemental videos:

Supplemental Video 1: Representative time-lapse video recording (z-projection) in a wild-type mouse with megakaryocytes extending proplatelet (green) within bone marrow sinusoids (red, Qtracker). Acquired with a Leica SP5 microscope equipped with a 12 kHz resonant scanner and a 25x water objective with a numerical aperture of 0.95 (Leica), z-stack acquisition at 10 s intervals, z-depth of 1.34 μm , x-y resolution 384 x 384 pixels, line averaging 8. Whenever necessary, the profile was aligned using the ImageJ template matching plug-in to obtain an average z-projection. Depending on the image quality, the background was subtracted, the image was smoothed, and the brightness and contrast adjusted.

Supplemental Video 2: Representative time-lapse video recording (z-projection) in a wild-type mouse with megakaryocytes extending proplatelet (green) within bone marrow sinusoids (red, Qtracker). Acquired with a Leica SP5 microscope equipped with a 12 kHz resonant scanner and a 25x water objective with a numerical aperture of 0.95 (Leica), z-stack acquisition at 10 s intervals, z-depth of 1.34 μm , x-y resolution 384 x 384 pixels, line averaging 8. Whenever necessary, the profile was aligned using the ImageJ template matching plug-in to obtain an average z-projection. Depending on the image quality, the background was subtracted, the image was smoothed, and the brightness and contrast adjusted.

Supplemental Materials:

Coding File 1: 3D printing–Block. 3D object file for the printing of the block.

Coding File 2: 3D printing–Skull ring. 3D object file for the printing of the skull ring.

Coding File 3: 3D printing–Support. 3D object file for the printing of the support.

Coding File 4: 3D printing–Screw ring. 3D object file for the printing of the screw.

DISCUSSION:

The mechanisms of platelet formation are highly dependent on the bone marrow environment. Hence, intravital microscopy has become an important tool in the field to visualize the process in real-time. Mice with fluorescent megakaryocytes can be obtained by crossing mice expressing the Cre recombinase in megakaryocytes with any floxed reporter mice containing a conditional fluorescent gene expression cassette. Here, mTmG reporter mice were used (B6.129(Cg)-*Gt(ROSA)26Sor*^{tm4(ACTB-tdTomato,-EGFP)Luo10}) crossed with Pf4-cre mice¹¹, allowing intense green fluorescence labeling in megakaryocytes and platelets¹². It is important to note that some leakage has been reported with Pf4-cre mice in leukocytes, including monocytes/macrophages and fibroblasts^{12,13}.

However, megakaryocytes are easily recognized by their large size and nucleus. Experimenters new to the field could compare observations in [mTmG; Pf4-cre] mice with those obtained after megakaryocyte-specific labeling. This is possible through intravenous administration of an Alexa-fluor-labeled antibody directed against the platelet-specific protein, GPIX (CD42a)^{3,14}. This latter

approach is also beneficial for imaging fluorescent megakaryocytes from any genetically engineered mouse without performing tedious and time-consuming mouse crossings with fluorescent reporter mice. Here, 5–7-week-old mice were used as younger mice present with a thinner bone that is more translucent and facilitates imaging compared to older mice. However, mice that are too young may present difficulties in the installation of the cranial ring without leakage.

In this study, intravital imaging was performed using a Leica microscope equipped with a 25x water objective with a numerical aperture of 0.95 (**Table of Materials**). The objective should be conical so that it can enter the cup formed by the cranial ring with an optimal working distance. Images were recorded with a resonant scanner (12 or 8 kHz). The overall settings will depend on the type of scientific question to be answered and should be optimized depending on the magnification, resolution, and acquisition speed needed. For instance, with a 12 kHz resonant scanner, a 25x objective would be better suited to measure platelet velocity, whereas an 8 kHz scanner and a lower magnification could be sufficient to record proplatelet elongation.

The most critical step of the protocol is the correct attachment of the ring to the skull bone so that no leakage occurs, and so that it does not detach during recording. For that, it is essential that the skull bone be dry just before applying the ring. Once the ring is glued, rapidly re-humidify the bone. Furthermore, due to the force exerted by the weight of the head on the ring, the ring is subjected to a tension that may cause it to detach partially during the recording. This may cause leakage and thus, dryness of the bone, leading to both poor-quality images and undesirable inflammatory reactions. This problem can be easily avoided by adding a folded compress under the nose of the mouse to support the head (**Figure 3C**). Another critical point is to minimize bleeding and the presence of blood inside the ring as it may lead to blurred images. This must be kept in mind when studying mice that present defective hemostasis and are prone to bleeding. Some tracers, such as dextran, may present leakage in the bone marrow cavity if injected in a concentrated form, which worsens vessel imaging, though not the green fluorescence of megakaryocytes. Qtracker-655 does not leak much but is cleared from the circulation within 30 min so that new injections of the tracer are required to visualize vessels over longer periods.

One limitation of this method described here is the necessity to stop acquisition every 35 min to re-inject anesthetics. This limitation can be overcome if an anesthesia machine is available. In that case, anesthesia can be induced similarly by i.p. injection of a mixture of ketamine and xylazine, which is the easiest way to perform the insertion of the catheter and the minor surgery. Once positioned below the microscope objective, anesthesia is then maintained by inhalation of gases (mixture of oxygen, anesthetics such as isoflurane and ambient air). In this way, observations can be made over several hours without interruption. However, for ethical reasons, observations were limited to 3 h in this study. Another limitation in using ketamine/xylazine mixture could be its potential deleterious impact on platelet functions¹⁶ that could require alternative anesthesia schemes.

Overall, the principal merit of this well-established protocol is its noninvasive aspect with only minimal surgery. Other protocols have been developed to perform time-lapse intravital imaging

in long bones. These rely on either invasive surgery that requires muscle tissue removal and bone abrasion^{17,18}, implanted endoscopic probes close to the femur head^{19,20}, or installing a window chamber in the femur²¹. All these procedures result in major trauma and varying degrees of inflammation. Inflammation is not only detrimental to the mouse, but it has also been reported to modify the process of platelet formation⁶ so that uncontrolled inflammatory conditions might lead to discrepancies and misinterpretation of the data. That is why this procedure was chosen to avoid inflammatory reactions. However, depending on the scientific question, experimenters may prefer to have a deeper observation field and higher resolution (less scattering), which is possible by using a skull-thinning-based approach at the expense of a low degree of inflammatory reaction.

Because of its noninvasive nature, the major limitation of this method is the maximal depth that can be reached. Due to the density of the bone and its scattering properties, it is possible to image regions within a depth of only a few hundred micrometers, preventing observations of the whole calvarial marrow. The development of three-photon microscopy, which relies on even higher infrared excitation wavelengths, seems to be a promising approach with superior deep-tissue resolution. It has already been successfully used to image deep into the brain even through the bone^{22,23}, opening up the exciting possibility to image bone marrow within long bones without having to thin the bone or implant a surgical window.

In summary, this method is increasingly used to study the behavior of megakaryocytes in the bone marrow and visualize the extension of proplatelets. In addition, by allowing the visualization of the outer calvarial compact bone as well as part of the underlying marrow, this method has already been used in many applications outside the platelet field. It has been used for the study of both bone and marrow cell dynamics in their environment, including osteoblasts and osteoclasts, leukocyte trafficking and marrow exit, endothelial cells and microvasculature architecture, blood flow dynamics in marrow microvessels, or cell homing²⁴.

ACKNOWLEDGMENTS:

The authors would like to thank Florian Gaertner (Institute of Science and Technology Austria, Klosterneuburg, Austria) for his expert advice on two-photon microscopy experiments at the time when we established the technique in the lab, Fabien Pertuy who began to set up this technique in the lab, and Yves Lutz at the Imaging Center IGBMC /CBI (Illkirch, France) for his expertise and help with the two-photon microscope. We also thank Jean-Yves Rinkel for his technical help and Ines Guinard for the drawing of the schema in Figure 1. We thank ARMESA (Association de Recherche et Développement en Médecine et Santé Publique) for its support in the acquisition of the two-photon microscope. AB was supported by post-doctoral fellowships from Etablissement Français du Sang (APR2016) and from Agence Nationale de la Recherche (ANR-18-CE14-0037-01).

DISCLOSURES:

The authors have no conflicts of interest to declare.

REFERENCES:

- 1 Junt, T. et al. Dynamic visualization of thrombopoiesis within bone marrow. *Science*. **317** (5845), 1767–1770 (2007).
- 2 Mazo, I. B. et al. Hematopoietic progenitor cell rolling in bone marrow microvessels: parallel contributions by endothelial selectins and vascular cell adhesion molecule 1. *Journal of Experimental Medicine*. **188** (3), 465–474 (1998).
- 3 Bornert, A. et al. Cytoskeletal-based mechanisms differently regulate in vivo and in vitro proplatelet formation. *Haematologica*. doi: 10.3324/haematol.2019.239111 (2020).
- 4 Zhang, L. et al. Sphingosine kinase 2 (Sphk2) regulates platelet biogenesis by providing intracellular sphingosine 1-phosphate (S1P). *Blood*. **122** (5), 791–802 (2013).
- 5 Kowata, S. et al. Platelet demand modulates the type of intravascular protrusion of megakaryocytes in bone marrow. *Thrombosis and Haemostasis*. **112** (4), 743–756 (2014).
- 6 Nishimura, S. et al. IL-1 α induces thrombopoiesis through megakaryocyte rupture in response to acute platelet needs. *Journal of Cell Biology*. **209** (3), 453–466 (2015).
- 7 Lefrancais, E. et al. The lung is a site of platelet biogenesis and a reservoir for haematopoietic progenitors. *Nature*. **544** (7648), 105–109 (2017).
- 8 Potts, K. S. et al. Membrane budding is a major mechanism of in vivo platelet biogenesis. *Journal of Experimental Medicine*. **217** (9), e20191206 (2020).
- 9 Scott, M. K., Akinduro, O., Lo Celso, C. In vivo 4-dimensional tracking of hematopoietic stem and progenitor cells in adult mouse calvarial bone marrow. *Journal of Visualized Experiments: JoVE*. (91), e51683 (2014).
- 10 Muzumdar, M. D., Tasic, B., Miyamichi, K., Li, L., Luo, L. A global double-fluorescent Cre reporter mouse. *Genesis*. **45** (9), 593–605 (2007).
- 11 Tiedt, R., Schomber, T., Hao-Shen, H., Skoda, R. C. Pf4-Cre transgenic mice allow the generation of lineage-restricted gene knockouts for studying megakaryocyte and platelet function in vivo. *Blood*. **109** (4), 1503–1506 (2007).
- 12 Pertuy, F. et al. Broader expression of the mouse platelet factor 4-cre transgene beyond the megakaryocyte lineage. *Journal of Thrombosis and Haemostasis*. **13** (1), 115–125 (2015).
- 13 Calaminus, S. D. et al. Lineage tracing of Pf4-Cre marks hematopoietic stem cells and their progeny. *PLoS One*. **7** (12), e51361 (2012).
- 14 Stegner, D. et al. Thrombopoiesis is spatially regulated by the bone marrow vasculature. *Nature Communications*. **8** (1), 127 (2017).
- 15 Drew, P. J., Blinder, P., Cauwenberghs, G., Shih, A. Y., Kleinfeld, D. Rapid determination of particle velocity from space-time images using the Radon transform. *Journal of Computational Neuroscience*. **29** (1–2), 5–11 (2010).
- 16 Nakagawa, T. et al. Ketamine suppresses platelet aggregation possibly by suppressed inositol triphosphate formation and subsequent suppression of cytosolic calcium increase. *Anesthesiology*. **96** (5), 1147–1152 (2002).
- 17 Kim, S., Lin, L., Brown, G. A. J., Hosaka, K., Scott, E. W. Extended time-lapse in vivo imaging of tibia bone marrow to visualize dynamic hematopoietic stem cell engraftment. *Leukemia*. **31** (7), 1582–1592 (2017).
- 18 Kohler, A., Geiger, H., Gunzer, M. Imaging hematopoietic stem cells in the marrow of long bones in vivo. *Methods in Molecular Biology*. **750**, 215–224 (2011).
- 19 Lewandowski, D. et al. In vivo cellular imaging pinpoints the role of reactive oxygen species in the early steps of adult hematopoietic reconstitution. *Blood*. **115** (3), 443–452 (2010).

- 20 Reismann, D. et al. Longitudinal intravital imaging of the femoral bone marrow reveals plasticity within marrow vasculature. *Nature Communications*. **8** (1), 2153 (2017).
- 21 Chen, Y., Maeda, A., Bu, J., DaCosta, R. Femur window chamber model for in vivo cell tracking in the murine bone marrow. *Journal of Visualized Experiments: JoVE*. (113), e54205 (2016).
- 22 Guesmi, K. et al. Dual-color deep-tissue three-photon microscopy with a multiband infrared laser. *Light Science & Applications*. **7**, 12 (2018).
- 23 Wang, T. et al. Three-photon imaging of mouse brain structure and function through the intact skull. *Nature Methods*. **15** (10), 789–792 (2018).
- 24 Kim, J., Bixel, M. G. Intravital multiphoton imaging of the bone and bone marrow environment. *Cytometry A*. **97** (5), 496–503 (2020).

Figure 1

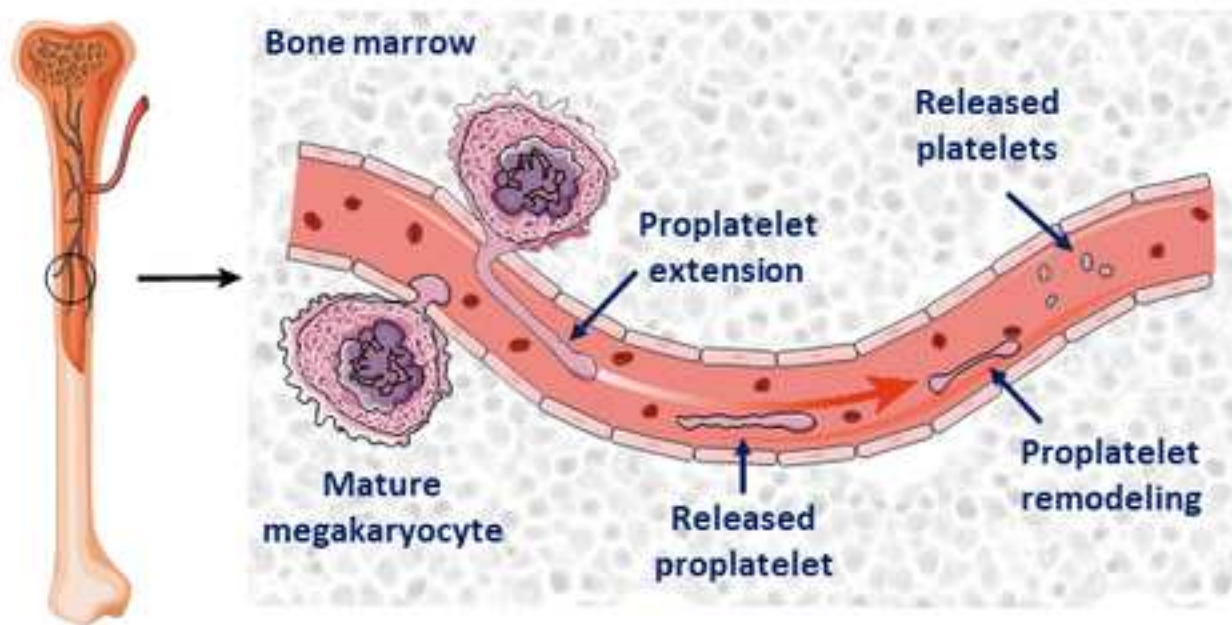


Figure 2

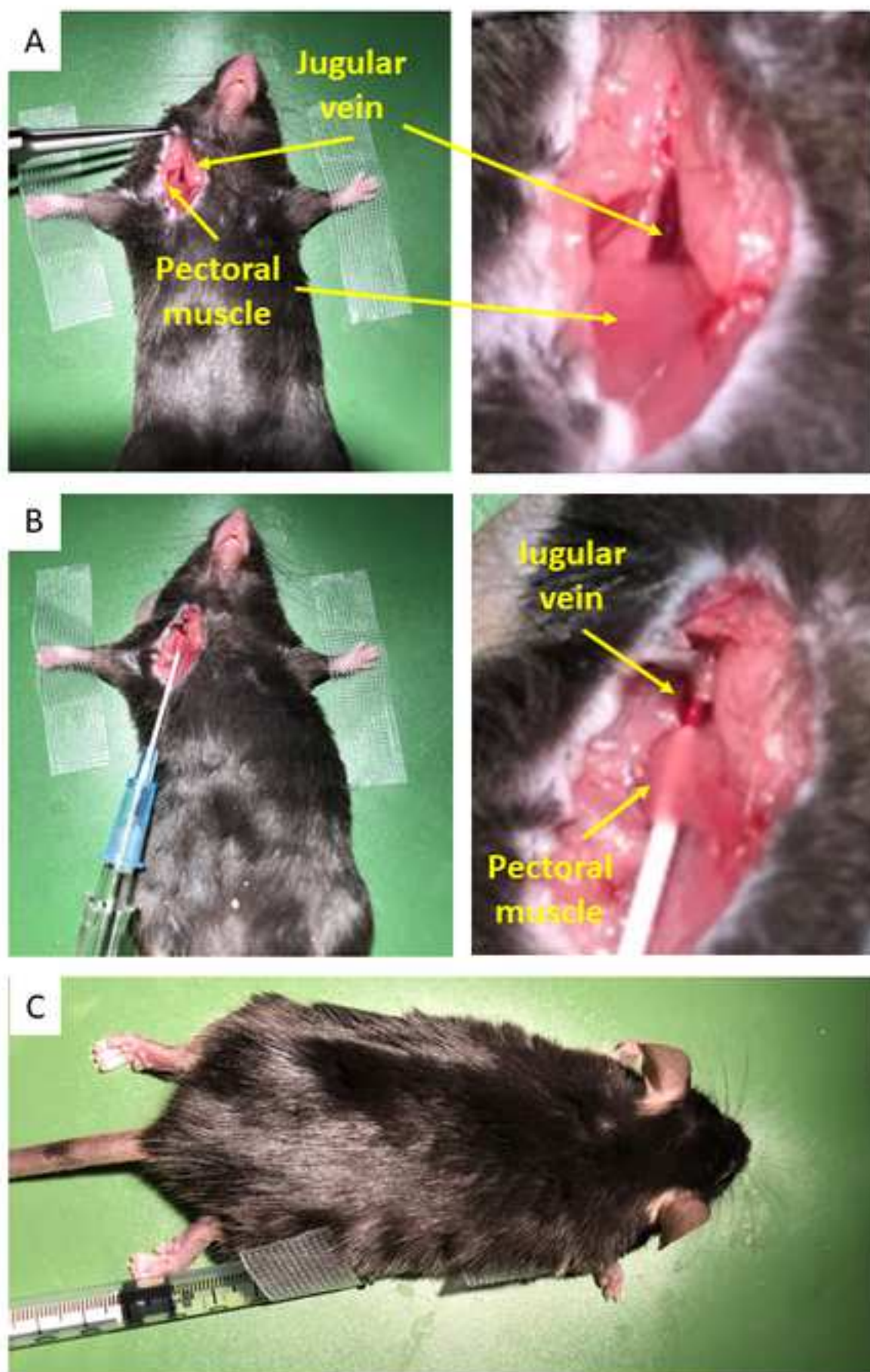


Figure 3

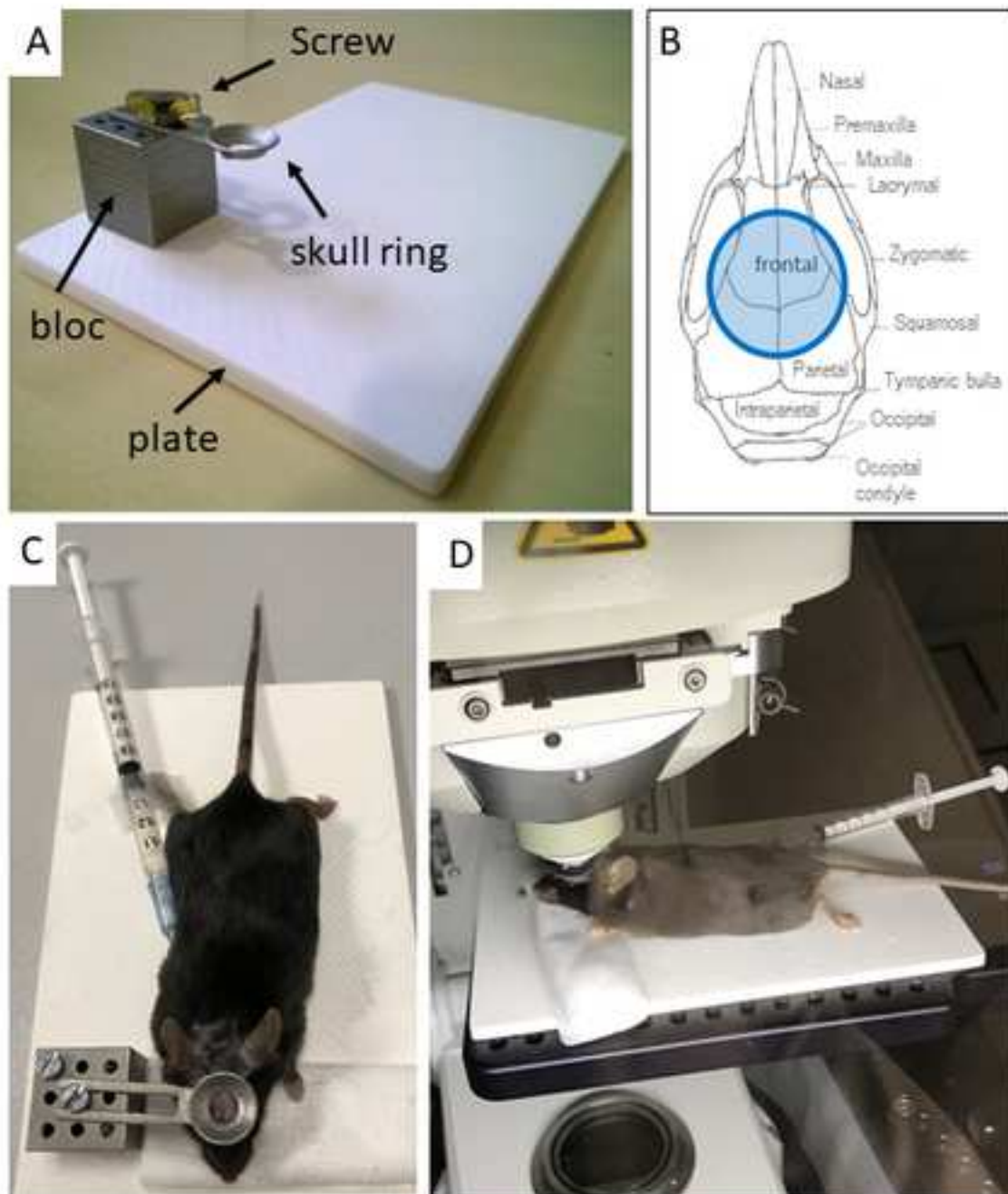


Figure 4

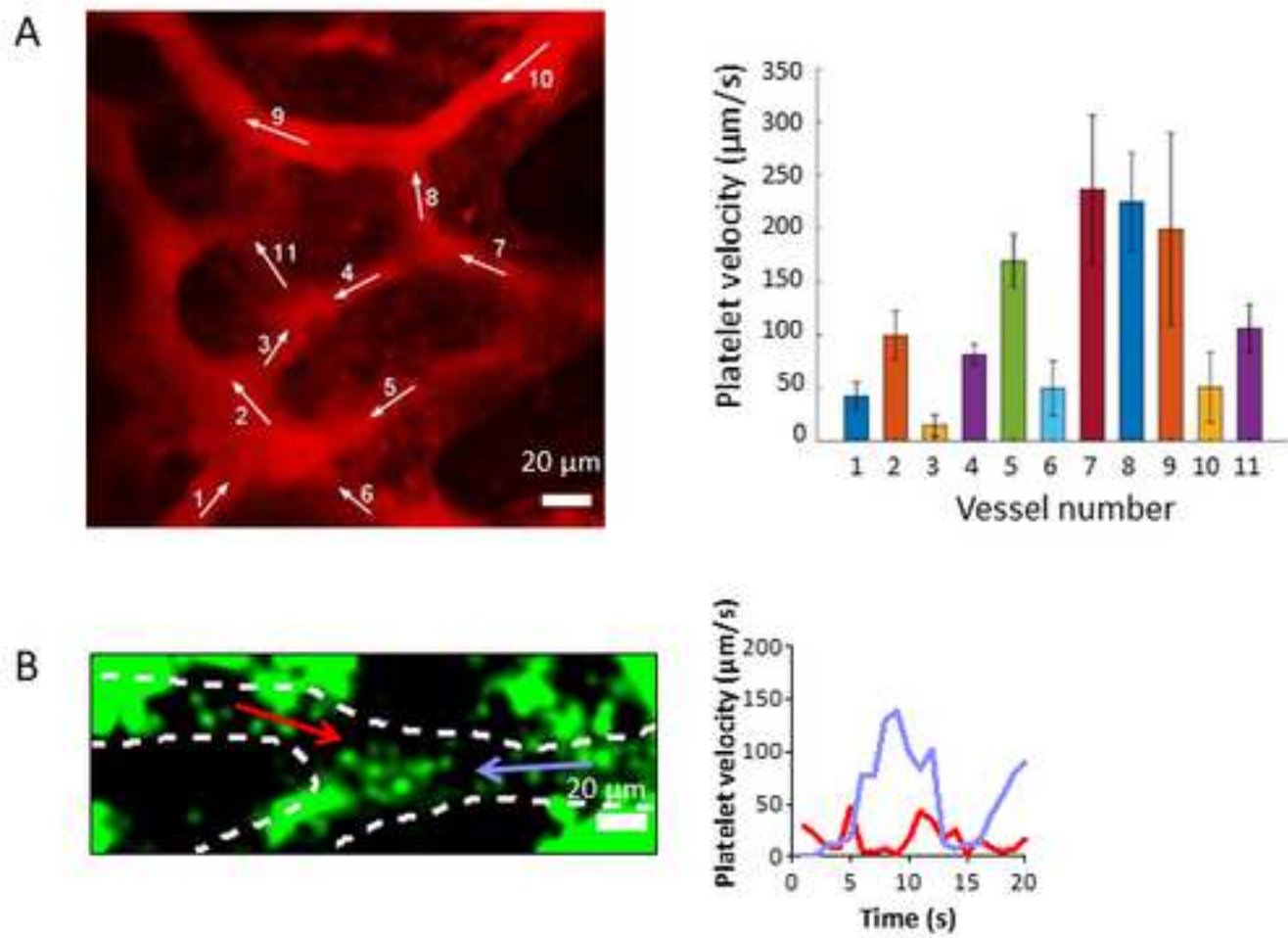


Figure 5

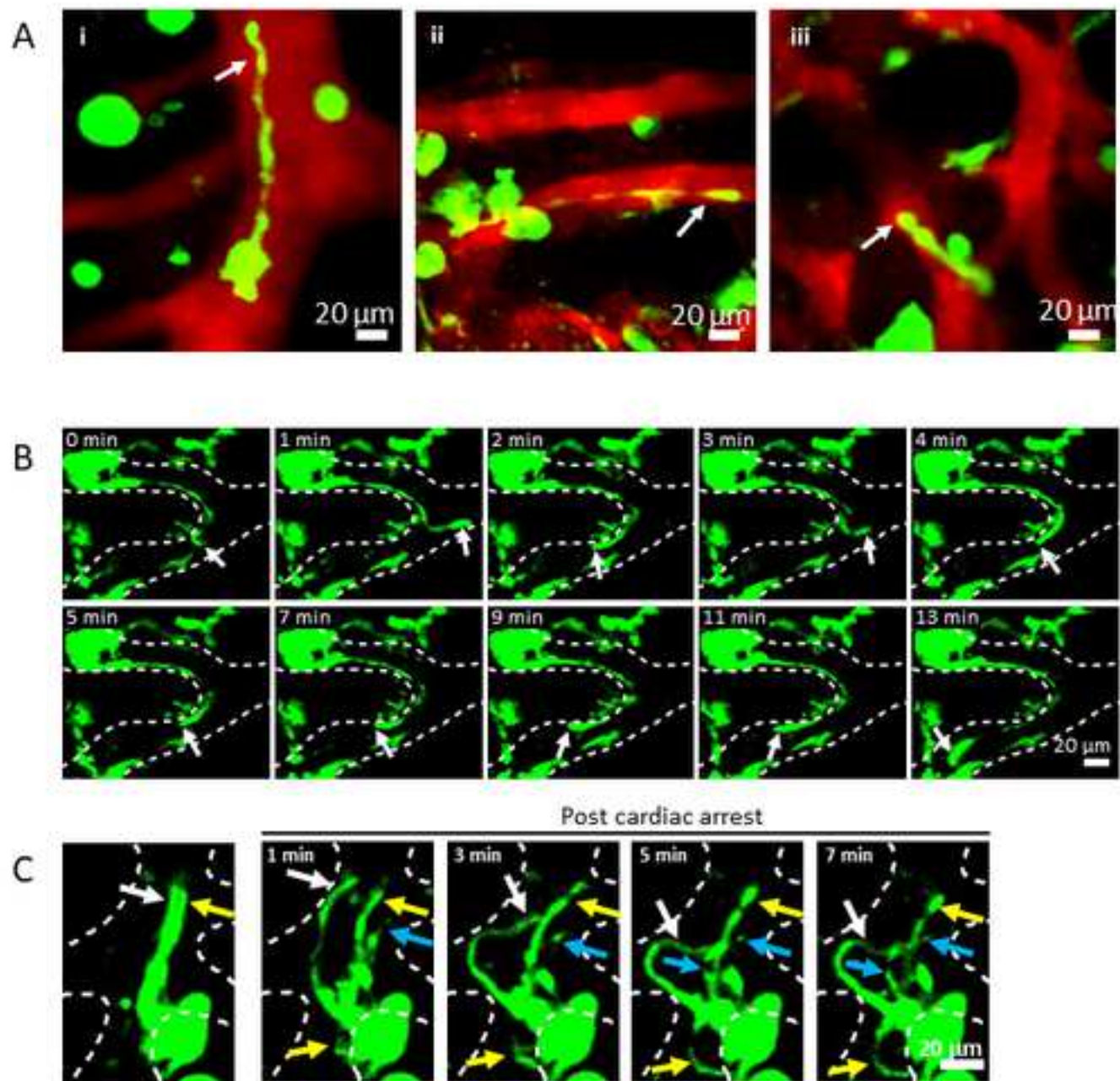
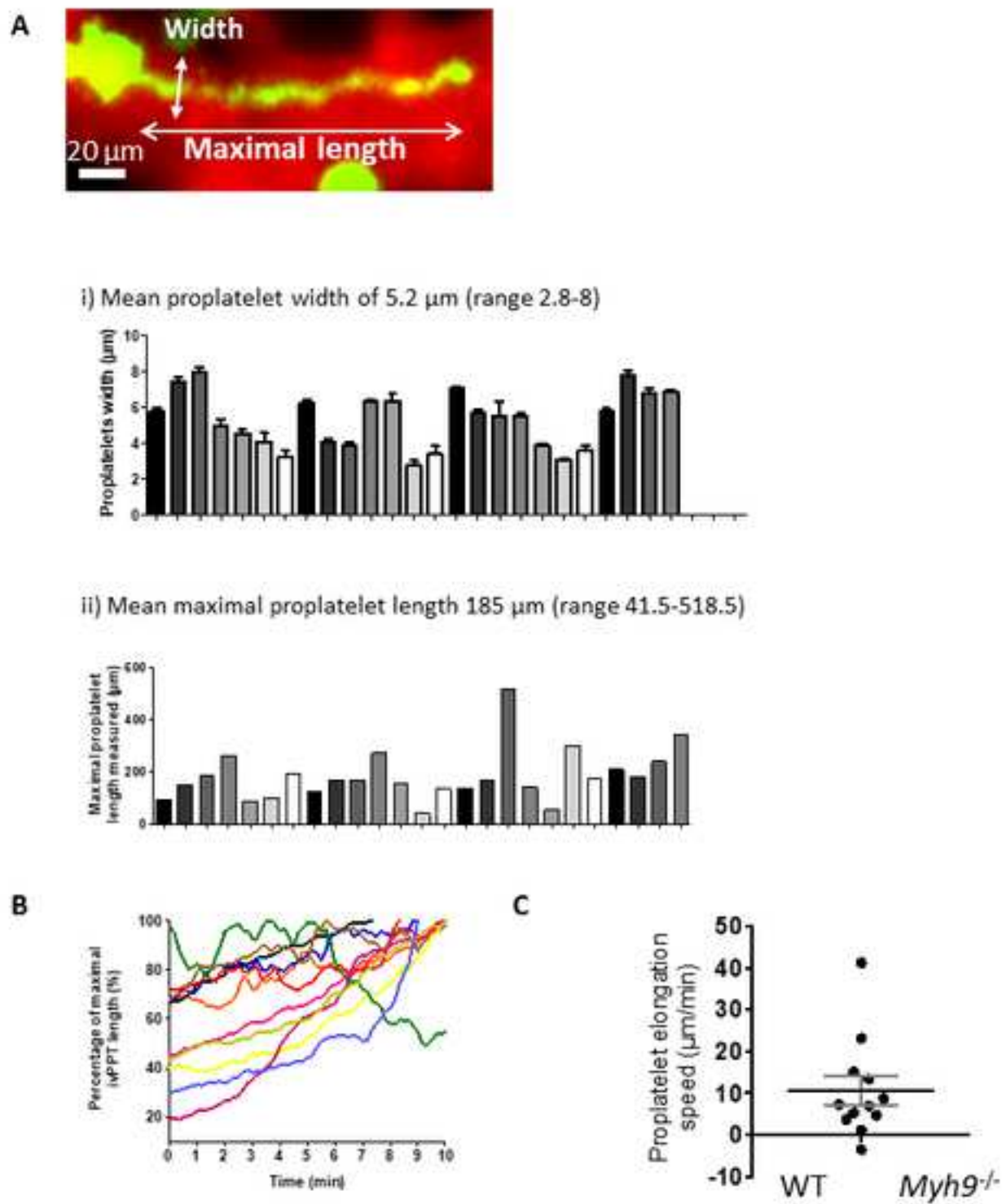
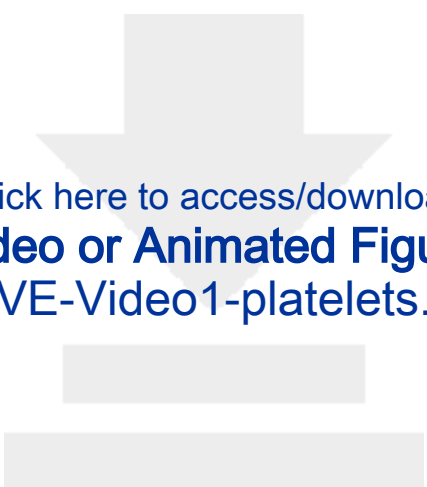


Figure 6

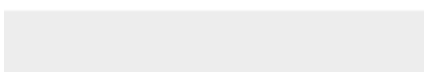




Click here to access/download
Video or Animated Figure
JOVE-Video1-platelets.avi



Click here to access/download
Video or Animated Figure
JOVE-Video2-PPTi.avi

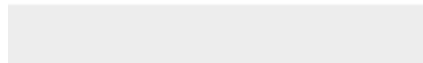




[Click here to access/download](#)

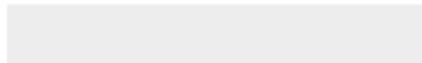
Video or Animated Figure

JOVE-Video3-PPT tossed.avi





Click here to access/download
Video or Animated Figure
JOVE-Video4-cardiac arrest.avi





Click here to access/download
Video or Animated Figure
JOVE-Video5-WT + vinc.avi

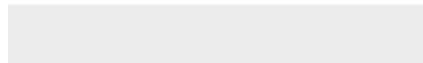




[Click here to access/download](#)

Video or Animated Figure

JOVE-Video6-ko Myh9 + vinc.avi



Name of Material/ Equipment	Company	Catalog Number	Comments/Description
GNU Octave software	GNU Project		https://www.gnu.org/software/octave/
Histoacryl 5 x 0, 5 mL	Braun	1050052	injectable solution of surgical glue
HyD hybrid detectors Leica	Leica Microsystems		
Microsystems 4tunes	GNU project		Minimum version required
ImageJ			
Imalgene/Ketamine 1000 fl/10 mL	Boehring	03661103003199	eye protection
Leica SP8 MP DIVE microscope equipped with a 25x water objective, numerical aperture of 0.95	Leica Microsystems		simultaneous excitation of AlexaFluor-488 and Qtracker-655
Matlab	MathWorks		https://www.mathworks.com/
Ocrygel 10 g	Laboratoires T.V.M.	03700454505621	Silicon dental paste blue and yellow
Picodent twinsin speed	Rotec	13001002	
Qtracker 655 vascular label	Invitrogen	Q21021MP	injectable solution
Resonant scanner, 8 or 12 kHz			
Rompun Xylazine 2% fl/25 mL	Bayer	04007221032311	
Superglue gel			to glue the ring to the bone
Surflo IV catheter - Blue 22 G	Terumo	SR-OX2225C1	
Ti:Saph pulsing laser (Coherent) (femtosecond)	Coherent		

Editorial comments AB

Answers to the reviewers

We thank the editor and the referees for reviewing our manuscript entitled “*In vivo* two-photon imaging of megakaryocytes and proplatelets in the mouse skull bone marrow”. All points raised by the editor and the reviewers have been addressed and the changes appear in the text in red. Please find below the detailed point-by-point answers to the comments.

Editorial comments:

Changes to be made by the Author(s):

1. Please take this opportunity to thoroughly proofread the manuscript to ensure that there are no spelling or grammar issues. Please define all abbreviations at first use.
2. Please provide an email address for each author.

The institutional email addresses have been provided.

3. JoVE cannot publish manuscripts containing commercial language. This includes trademark symbols (™), registered symbols (®), and company names before an instrument or reagent. Please remove all commercial language from your manuscript (text, figure legends, figures, tables) and use generic terms instead. All commercial products should be sufficiently referenced in the Table of Materials and Reagents. This has been done.

For example: Alexa fluor; Qtracker™655 vascular labels (Invitrogen); Matlab etc

4. Being a video based journal, JoVE authors must be very specific when it comes to the humane treatment of animals. Regarding animal treatment in the protocol, please add the following information to the text:

a) Please specify the euthanasia method without highlighting it.

As requested by the editor, this specification has been added in the protocol section.

b) For survival strategies, discuss post-surgical treatment of animal, including recovery conditions and treatment for post-surgical pain.

Mice are euthanized before recovery. This specification has been added in the protocol section.

c) Discuss maintenance of sterile conditions during survival surgery. We have added a note lines 137-140.

d) Please specify that the animal is not left unattended until it has regained sufficient consciousness to maintain sternal recumbency.

e) Please specify that the animal that has undergone surgery is not returned to the company of other animals until fully recovered.

For point d and e, mice are euthanized before recovery. This has been added in the manuscript.

5. Please revise the text, especially in the protocol, to avoid the use of any personal pronouns (e.g., "we", "you", "our" etc.). [This has been done.](#)

6. Please note that your protocol will be used to generate the script for the video and must contain everything that you would like shown in the video. Please add more details to your protocol steps. Please ensure you answer the "how" question, i.e., how is the step performed? Alternatively, add references to published material specifying how to perform the protocol action. Please add more specific details (e.g., button clicks for software actions, numerical values for settings, etc) to your protocol steps. There should be enough detail in each step to supplement the actions seen in the video so that viewers can easily replicate the protocol.

[We have especially added details regarding the analysis of morphological parameters and velocity.](#)

7. After including a one line space between each protocol step, highlight up to 3 pages of protocol text for inclusion in the protocol section of the video. This will clarify what needs to be filmed.

[This has been done.](#)

8. Please include a scale bar for all images taken with a microscope to provide context to the magnification used. Define the scale in the appropriate Figure Legend. [The scale is present and defined in each image taken with the microscope.](#)

9. Please include all video and other supplemental file legends in the figure and table legends section and make sure that the reader understands from the references in the text when to refer to these and what to expect. [This has been done.](#)

10. Please do not abbreviate journal names. [I did not manage to modify in the output style of EndNote. If required, I will do it manually on references converted to plain text.](#)

11. Please sort the Materials Table alphabetically by the name of the material. [This has been done.](#)

Reviewers' comments:

Reviewer #1:

Manuscript Summary:

The manuscript by Bornert et al. is well written and describes in detail the experimental procedure needed to image in vivo the dynamic behavior of megakaryocytes and the formation of proplatelets using two-photon imaging and a cranial window technique. The authors relate the presented procedure to other imaging protocols used in the field and explain the strengths and limitations.

Major Concerns:

None

Minor Concerns:

p. 32-33: in vivo or living mice (one word redundant, use one or the other). [OK](#)

p. 55 The different mechanisms that in vivo proplatelet formation rely on compared to in vitro should be specified in more detail. [We have added a sentence to explain.](#)

p.83: The insertion of a catheter into the jugular vein seems to be a quite invasive procedure and it is not clear why tail vein injection is not the method of choice. It is later mentioned that tail vein

injection is also an option, but a fewer volume could be injected through this route. How much is the difference in volume that can be injected? Wouldn't be a less invasive injection route better and using higher concentration of the tracer or applied drug ? How can complications from bleedings during the insertion of the catheter/needle be addressed?

We agree with the reviewer that insertion of the catheter into the jugular vein is more invasive as tail vein injection as such. However, in our experience, inserting the catheter into the jugular vein is more reliable as it is first easier to set up due to the larger caliber of the vein compared to that of the tail, and less susceptible to be displaced upon manipulation of the mouse or when changing the syringe or when performing several successive injections. Inserting a catheter into tail vein is less easy due to its smaller caliber, especially in black mice where they are less visible. Hence it requires lots of practice and a pre-heat step of the tail to dilate the veins. We have specified this point line 161.

In our experience, placing catheter through the jugular vein do not lead to bleedings even in mice having hemostasis defects (such as integrin beta3 ko mice), because the pectoral muscle exerts a sufficient compression point. We have specified this point line 155-156.

By comparison, several unsuccessful attempts through tail vein resulted in bleedings (though minor) in integrin beta 3 deficient mice.

p.89: Measuring the blood flow velocity from the platelet movement assumes that the platelets are moving with the same velocity as the blood. The proplatelets are long and thin and might more likely move slower, while the smaller platelets might flow with the same velocity as the blood. This problem should be briefly addressed. We indeed measured platelet velocity and assume that it may represent blood velocity. For sure, platelet velocity gives an indication of the acceleration, deceleration and direction of the blood flow. Proplatelets which we observed are still attached to the stationary megakaryocyte, hence they do not move as a whole but they elongate, and we measured the elongation velocity. The mechanisms for elongation is complex, relying on both the blood flow that contributes through the drag force, the presence of contractile forces that tend to retract the proplatelets, and also the way the DMS membrane reservoir fuse with the plasma membrane to allow very long extension before rupture. Once the proplatelet has ruptured from its mother cell (anchorage point), it disappears in the flowing blood so that it is hardly possible to measure its velocity. We have added this point lines 446-448.

p. 184-185, 190: Reference to Fig. 3E-G is cited, but there is no 3E-3G in figure 3 (not in figure legends nor in the image). It was indeed Fig. 3C, we have corrected this error.

p. 275: It is not clear based on which method or formula the flow velocity is calculated. Reference to Matlab or GNU Octava software doesn't explain it.

The velocity of the platelets in the blood flow is estimated from the space-time images using a computational analysis based on the Radon transform described by Drew and collaborators (2010). The description of this mathematical method is beyond the scope of this review and the reader is referred to the publication by Drew and coll. for details regarding the calculation. These authors have made the code available in their website (mentioned in the manuscript), which, when opened through Matlab, allows the calculation of velocity. We have modified this section, hoping it is now more easily understandable.

p. 207: The leakage of vascular tracer into the BM cavity is not addressed, especially during prolonged imaging. I would assume that tracer leakage worsens the image quality over time.

Some tracers such as Dextran may indeed leak in the BM cavity. However, the main issue with the Qtracker vascular tracer is its disappearance over time, due to clearance from the circulation, rather than its leakage into the BM cavity. To circumvent this problem, the tracer can be reinjected (but this implies to pause the recording and open the imaging chamber). However, even in case of leakage, it does not worsen the image quality of the green (GFP/AF-488 fluorescent MKs). We have added a note to mention these problems, lines 277-281.

Figure 2: A zoom-in image how to place and insert the catheter would be helpful.

A zoom-in image has been added.

Reviewer #2:

1. The protocol described in the manuscript is of interest of scientists that investigate location of megakaryocytes, proplatelets and platelets production.
2. The introduction of the protocol is sufficient. All the steps are described in details and comprehensible.
3. The manuscript is well written.

Comments:

Increasing data points on megakaryocytes and their derivatives, such as platelets and microparticles, to be important in immune response towards inflammation. Hyperinflammation of cytokine storms and sepsis strongly affects coagulation and thrombosis. We still do not know much about the exact locations of megakaryocytes occurrence and platelets production. Imaging of megakaryocytes' location, movements and behavior can give a good answer to all these issues.

We thank the reviewer for his encouragements.

Reviewer #3:

Manuscript Summary:

The authors describe their method for achieving detailed in vivo fluorescent imaging of platelet production dynamics from Megakaryocytes, in bone marrow of the skull. The basic description of the surgery is nicely detailed and I presume will be well illustrated in the video version. The authors provide beautiful imaging to support the power of their approach. I specifically want to laud the authors for provision of stl files for 3D printing of the various components needed for their approach. This is a fantastic and oft overlooked element of publications of this sort. In general this is an approach well-worth inclusion and production of a video for a JOVE publication however a few major and minor points should be noted with respect to the uniqueness of this approach relative to other previous JOVE publications, inclusion of critical technical details, and discussion of caveats.

Major Concerns:

Uniqueness of this method:

Not referring to novelty of approach here but rather how this method is distinct from other methods previously published in JOVE. In particular, (<https://www.jove.com/t/51683/in-vivo-4-dimensional-tracking-hematopoietic-stem-progenitor-cells>) which uses a largely identical minor surgery based cranial window.. This isn't an issue for this type of publication - however - it would be nice to emphasize what makes this described method specific with respect to the analysis of megakaryocytes and platelets.

We have mentioned the previous paper and specified that here we evaluated megakaryocytes and platelets (line 85-88).

Why for example is a minimally invasive technique like this specifically be of great utility in study of platelets as compared to a microfracture or skull thinning based approach.

We have also added in the discussion the interest to use this poorly invasive technique (to prevent as far as possible undesirable inflammatory reactions) compared to other ones including skull thinning (lines 426-430).

With this in mind a greater emphasis on the downstream analytical/computational tools presented would be very valuable to readers and adopters of the approach. Currently this section is fairly thin in the overall method.

We have detailed this part, notably the way used to measure proplatelet maximal length and width with imageJ.

Specificity of Cre system indicated:

Use of the Pf4-cre system and mTmG is well established for intravital microscopy experiments however in this system (Pf4-cre), Cre can be variably expressed in other cell lineages, in fact this is true of PF4 mRNA and protein as well (notably certain myeloid cells of the immune system). Please provide one to two sentences to discuss these considerations with respect to how a researcher can be certain they are examining megakaryocytes in their in vivo analysis.

We agree with the reviewer that the Pf4-cre model presents leaks outside the megakaryocyte lineage and we notably published that some leucocytes as well as some fibroblasts and macrophages may be recombined and appear green. And this recombination is emphasized under inflammatory conditions (Pertuy et al., 2014). In the bone marrow, megakaryocytes are recognized by their location close to the sinusoid vessels and their large size (immature MKs do not express much eGFP), and large polylobed nucleus (the nucleus appears black surrounded by green on one focal plane). Comparison with 2-photon using a megakaryocyte specific marker (eg. Anti-GPIX antibody) may be recommended for newcomers in the field. We have added this point lines 110-116.

Anesthesia: Repeat dosing with Ketamine/Xylazine is a slight departure from most (though not all) sustained intravital microscopy systems. Authors note this in the discussion but a relevant "Note:" in the main description would be appropriate.

We have added this in a note, line 128-132.

Potentially a greater issue is Ketamine has been reported to suppress platelet function (notably aggregation), this may not impact the types of studies described by the author (platelet velocity) but it is a caveat to the anesthetic choice and certainly worth mentioning and citing the relevant literature as this is an area where researcher may choose alternate anesthesia schemes to better fit with their intended purposes.

We have mentioned this point in the discussion, lines 601-603. However, having a strong expertise in platelet function in the lab, including in platelet aggregation, we never observed impacts of the mixture ketamine/xylazine used to anesthetized the mice via i.p. on platelet rich plasma aggregation, in comparison to aggregation performed in washed platelets where plasma and potential anesthetics are removed. In fact, the ketamine injected as i.p. (reaching around 8 μmol per 20g mouse) is probably highly diluted when reaching the blood circulation. By comparison, Nakagawa et al. uses 250 μM -1 mM directly added to the PRP.

Microscope Specifications:

Many critical features of the microscope this approach is performed on are either buried in the text or completely unreported. This is essential information as things like objective specifications (Magnification, Numerical Aperture, etc...) and frequency of the resonant scanner dictate many aspects that the authors note as optimal imaging criteria -

For example:

3.7.2 - "We usually used line averaging of 8, which allowed acquisition of 1 image/10 s. "

Rate at which a single line can be collected is dependent on the frequency of the scanner but this isn't reported until 3.7.3.6 (as an off-hand note)

[This specification has been added.](#)

3.7.2 - "For long acquisitions (eg. Visualization of proplatelet formation or elongation), acquire z-stack images at 1.34 μm intervals using resonant scanner. We usually acquired 384x384 pixel images to visualize the entire megakaryocyte and vessel. "

The pixel values are essentially meaningless without knowledge of the objective and scanner.

I'd suggest including a description at the beginning of the two-photon section that described the specifics of the microscope this work was performed on,

[We agree with the reviewer and have added microscope specifications at the beginning of the Two-photon imaging section.](#)

and more importantly what of these specifications are essential for this method to work. E.G. do you need a 12 kHz scanner to effectively capture the biology in question or would an 8 kHz scanner work just as well. Can you effectively perform this technique with a 16x objective (relatively inexpensive) or do you really need a very high NA 25x objective (very expensive) to be able to perform this type of analysis. Are hybrid detectors critical to this approach or can you get away with a standard PMT.

[The use of a 16x vs 25x objective depends on the magnification/resolution required. In our case, as we also wanted to follow individual platelets, we found that the 25x objective was required. We have mentioned this. However, we did not compare our data with that obtained using a classical PMT.](#)

Bullet points hard to follow:

This may be easier when considering the video but the logical flow of the bullet points between 3.7.2 and 3.7.3.6 is all over the place bouncing around between anesthesia application (or re-application) and "minimize Z-stack to increase acquisition rapidity". I would find it much more logical to focus on

a single run and the considerations there. And then provide a second section discussing alterations of the approach for other purposes (e.g. "Minimize (eg. 256x90 pixels) and adjust image size to the vessel by rotating the imaging field if required. "

We agree with the reviewer and have now added a new section 3. "Follow up of the anesthetized mice". We have also separated long acquisitions "section 4.7" from short and rapid acquisitions "section 4.8".

Also for a broad audience like JOVE probably not a bad idea to explain what bidirectional scanning, phase adjustment, line averaging, etc... actually mean.

We have better explained these terms lines 254-256.

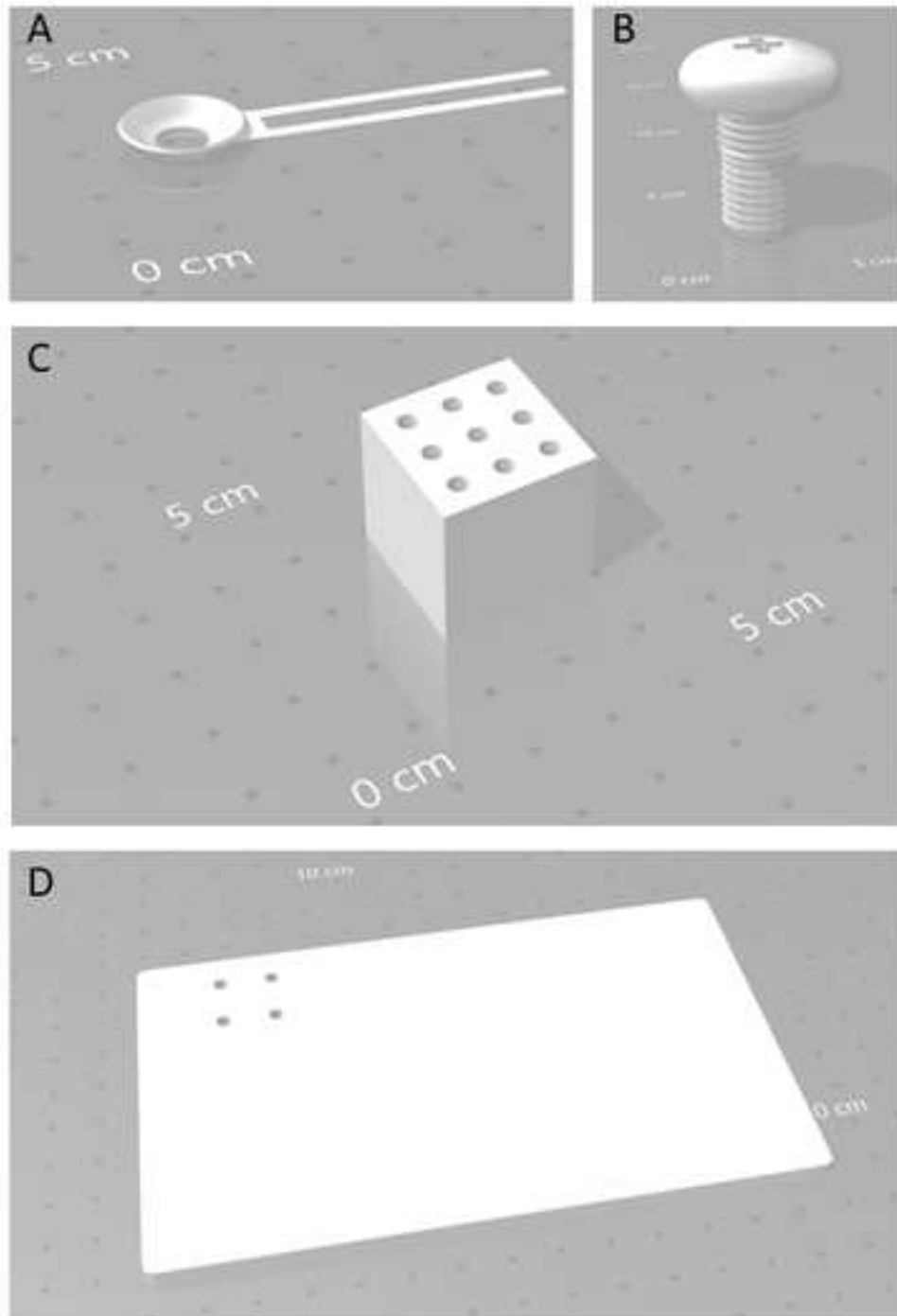
Minor Concerns:

Minor: Grammar/Spelling pass. Overall manuscript is very well written however a slightly more than average number of grammatical errors snuck through - Would recommend having a solid copy-editor make a pass at this before publication.

We have tried to remove as far as possible the grammatical errors.

- Change light surgery to "minor" surgery

This has been changed.





[Click here to access/download](#)


Supplemental Coding Files

3D printing - Bloc (Stainless steel).stl





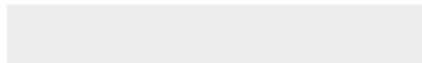
Click here to access/download
Supplemental Coding Files
3D printing - screw ring.stl

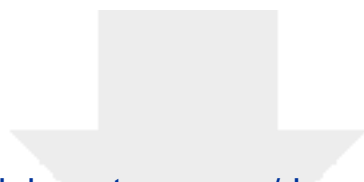




[Click here to access/download](#)

Supplemental Coding Files
3D printing - Support (ABS).stl

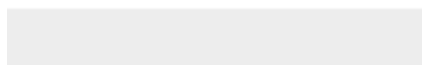


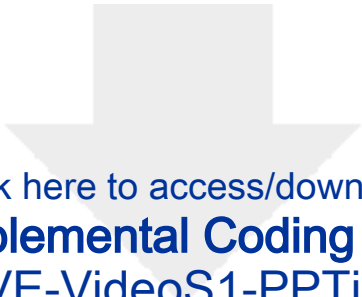


[Click here to access/download](#)

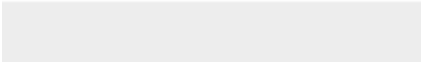

Supplemental Coding Files

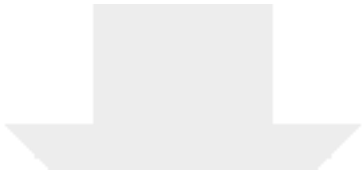
3D printing - Skull ring (High detailed stainless steel).stl





Click here to access/download
Supplemental Coding Files
JOVE-VideoS1-PPTii.avi





Click here to access/download
Supplemental Coding Files
JOVE-VideoS2-PPTiii (1).avi

